Effect of a non-Maxwellian component of the neutron flux in the determination of minor actinide thermal cross sections

A. Letourneau, F. Marie, D. Ridikas
CEA/Saclay - DSM/DAPNIA/SPhN - FRANCE

August 28, 2003

1 Introduction

The aim of the present document is to summarize recent quantitative studies of the effect of a non-Maxwellian neutron flux component in the measurement of thermal neutron cross sections (Maxwell averaged or at $E_n = 0.0253\ eV$), in highly thermalized neutron spectra. The studies presented here have been performed on minor actinides whose nuclear parameter measurements show a demonstrated interest for the transmutation of the nuclear wastes [1, 2, 5]. We focalize our interest to the proposed or realized measurements in the frame of the Mini-INCA project at the HFR of ILL-Grenoble [6, 7]. Thermal neutron capture and fission cross sections are measured in two experimental neutron channels where different measurement techniques are operational:

- the H9 super-thermal channel where capture and absorption cross sections are measured, thanks to off-line γ and α spectroscopy performed on irradiated samples.
- the V4 variable spectrum channel where online fission rates are measured with micro-fission chambers. Sample activation experiments followed by mass spectrometry are also performed off-line.

We present the contributions of non-thermal neutrons to the measured capture and fission cross sections and the correction factors to be applied to the results, depending on the actual neutron energy spectrum. This study lay on new high statistic simulations of the neutron flux based on the MCNP modelization of the ILL reactor [4]. Six irradiation positions have been studied :

- the nominal irradiation position in the horizontal H9 channel (at $\sim 50\ cm$ from the fuel element), providing a 98% thermalized ($50°C$) neutron flux with a total intensity of $6.10^{14}\ n/s/cm^2$.
- positions at 0, 25, 50, 75 and 100 cm from the bottom of the vertical inclined (V4) channel, corresponding to the nominal fission chamber irradiation positions. The bottom position is at $\sim 10\ cm$ from the fuel element and provides a 84% thermalized neutron flux with a total intensity of $1.6\ 10^{15}\ n/s/cm^2$

2 Experimental approach

2.1 Neutron flux simulations

The following results are based on high statistics ($5.10^6 to 20.10^6$ fission neutrons) MCNP simulations of the ILL neutron flux at different irradiation positions. These simulations are based on a precise modelization of the HFR core [4] that reproduce correctly the history of the fuel cycle of 50 days. Neutron flux simulations with a statistical accuracy better than 1% have been performed at the 6 most widely used irradiation positions by the Mini-INCA project :

- H9 channel
- V4 channel at 0, 25, 50 75 and 100 cm from the bottom position

Those simulations have been done with two sets of cross section libraries prepared at two different temperatures (30° C and 130° C) for the D_2O moderator in order to interpolate the effective neutron energy distribution at the averaged temperature of the moderator: $T = 50°\ C$
The calculated flux intensities and the proportion of thermal neutron in the total flux are presented in table 1 and figure 1. Simulation of the neutron flux inside the fuel element (core) is also given here for comparison. As shown in the table, there is no significant difference in the fluxes calculated at $T = 30°\ C$ and $T = 130°\ C$.

Flux	ϕ^{30}	$\frac{\phi^{30}_{th}}{\phi^{30}}$	ϕ^{130}	$\frac{\phi^{130}_{th}}{\phi^{130}}$
core	0.2210E+16	0.1048	0.2232E+16	0.1114
V4(0)	0.1712E+16	0.8418	0.1706E+16	0.8440
V4(25)	0.1356E+16	0.8971	0.1350E+16	0.8987
V4(50)	0.7301E+15	0.9686	0.7348E+15	0.9643
V4(75)	0.2893E+15	0.9966	0.3001E+15	0.9974
V4(100)	0.9645E+14	1.0000	0.9962E+14	1.0000
H9	0.6781E+15	0.9811	0.6818E+15	0.9806

Table 1: *ILL neutron flux simulations for 2 different neutron temperatures of* $30°C$ *and* $130°C$. *The proportion of thermal neutrons is obtained by integrating the neutron flux corresponds in the range* $0 < E_n < 1\ eV$.

2.2 Non-thermal neutron contribution

Due to the high level of neutron thermalization at ILL, the integral cross sections measured are generally presented in term of Maxwell averaged cross sections at the temperature of the D_2O moderator : $T \sim 50°C$.
Assuming a $\frac{1}{\sqrt{E_n}}$ behavior of the cross sections at low energy, one generally derives the thermal cross sections σ_0 at $E_n = 0.0253\ eV$ $(T = 293°K)$ from the Maxwell averaged

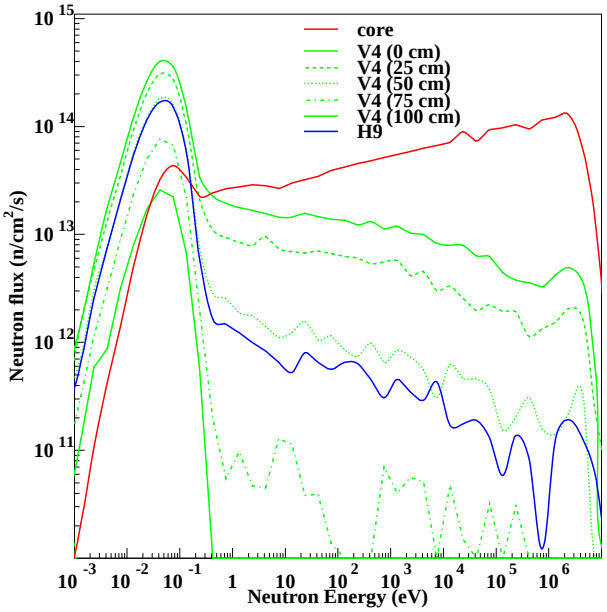

Figure 1: *Flux intensities expressed in $n/s/cm^2$ for logarithmic bins of energy, calculated for various positions in the HFR core.*

cross sections $< \sigma >^{T}_{Max}$ at temperature T, with the following formula :

$$\sigma_0 =< \sigma >^{T}_{Max} \times \sqrt{\frac{T}{293}} \times \frac{2}{\sqrt{\pi}} \tag{1}$$

Note that in H9, the hypothesis of a Maxwellian flux is relevant and confirmed by Monte-Carlo calculations of the flux at $30°C$ and $130°C$, showing that the simulated fluxes fit very well Maxwellian distributions (cf fig 2) at low energy.
However, the complementary non-Maxwellian component of the flux, can play a non-zero role due to the presence, in some cases, of huge resonances close to the thermal region. The contribution of the epi-thermal (non-Maxwellian) distribution to the averaged cross section could therefore be non-negligible, even if the epi-thermal component of the flux represents only a few percents of the total neutron intensity.
The averaged cross section is defined in the following way:

$$< \sigma >= \frac{\int_0^\infty \sigma(E).\phi(E)dE}{\int_0^\infty \phi(E)dE} \tag{2}$$

where $\sigma(E)$ is the differential cross section derived from the evaluations, and $\Phi(E)$ the calculated neutron spectrum. This equation can be discretized using the neutron intensity Φ_i in the energy bin i, instead of flux density $\phi(E)$, and divided in two separate terms: thermal and epi-thermal.

$$< \sigma > \quad = \quad \frac{\sum_i^{nbin} \sigma_i.\Phi_i}{\sum_i^{nbin} \Phi_i} \tag{3}$$

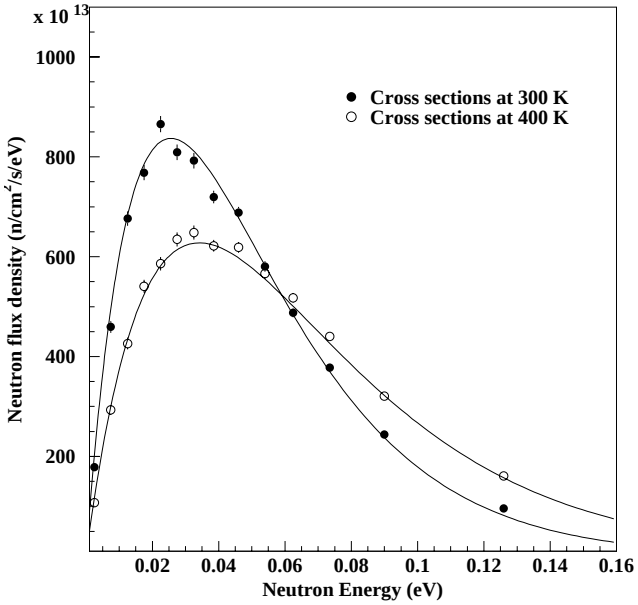

Figure 2: *Fit of the thermal component of the neutron fluxes in H9 calculated with MCNP (symbols) and cross section libraries prepared at* $30°C$ *and* $130°C$*, with Maxwell averaged distributions (continuous lines).*

$$= \frac{\sum_i^{th} \sigma_i.\Phi_i + \sum_j^{epi} \sigma_j.\Phi_j}{\Phi} \quad (4)$$

$$\simeq < \sigma >_{Max} \frac{\Phi_{th}}{\Phi} + < \sigma >_{epi} \frac{\Phi_{epi}}{\Phi}, \quad (5)$$

assuming $< \sigma >_{Max} = < \sigma >_{th}$.
From the last relation one can calculate the ratio between the experimental cross section and the Maxwell average cross section:

$$\frac{< \sigma >}{< \sigma >_{Max}} = 1 - \frac{\Phi_{epi}}{\Phi} \left(1 - \frac{< \sigma >_{epi}}{< \sigma >_{Max}}\right) \quad (6)$$

This equation shows that the hypothesis $< \sigma > = < \sigma >_{Max}$ is satisfied only by two conditions: either the epi-thermal component of the flux is negligible or epi-thermal and thermal averaged cross sections have the same values. Depending on whether the shape of the neutron spectrum and the shape of the cross sections, a correction factor will have to be applied to extract correctly the thermal cross sections from the data measured.

2.3 Cross section determination

Actually, the determination of these coefficients is a bit more complex as cross sections measured in H9 or V4 at ILL are generally determined in comparison with reference materials (flux monitors or reference deposits) irradiated in the same conditions as the actinide samples, and chosen for their well known cross sections:

- ^{59}Co for capture and absorption cross sections in H9
- ^{93}Nb for capture and absorption cross sections in V4
- ^{235}U for fission and absorption cross sections in V4 (with fission chambers)

In this scheme, what actually account is not the amplitude of the correction for a given isotope, but how it compares to the reference material correction factor.
We present here the analysis method. Particularly, one can be convinced that the determination of Φ is implicit, leading to an averaged measured cross section for isotope X expressed as a function of a reference averaged cross section for isotope Ref:

$$< \sigma(X) >= \frac{\alpha(X)}{\Phi} = \frac{\alpha(X)}{\alpha(Ref)} \times < \sigma(Ref) > \tag{7}$$

where, α for isotope X and Ref, depend only on experimental parameters (masses, counting rates, detection efficiencies, duration of irradiation, etc...). The thermal cross sections (Maxwell averaged and σ_0) can thus be derived from the measurements with these relations:

$$< \sigma(X) >_{Max} = \frac{\alpha(X)}{\alpha(Ref)} \times < \sigma(Ref) >_{Max} \times \left(\frac{\Lambda_{Max}(Ref)}{\Lambda_{Max}(X)} \right) \tag{8}$$

where, $\Lambda_{Max} = \dfrac{< \sigma >}{< \sigma >_{Max}}$ are the correction factors determined by Monte-Carlo simulations. Note that if equation 1 isn't verified (due to the effect of closed resonances), thermal cross section σ_0 has to be extracted with:

$$\sigma_0(X) = \frac{\alpha(X)}{\alpha(Ref)} \times \sigma_0(Ref) \times \left(\frac{\Lambda_0(Ref)}{\Lambda_0(X)} \right) \tag{9}$$

and $\Lambda_0 \neq \Lambda_{Max}$.

2.4 Calculation of averaged cross sections

We have determined the averaged cross sections from the interpolation of averaged cross sections calculated at $30°C$ and $130°C$. Using a linear hypothesis, we can thus derive the averaged cross section at the actual temperature of the moderator ($50°C$):

$$< \sigma >_{50} \simeq < \sigma >_{30} + \frac{\Delta < \sigma >}{5} \quad , \tag{10}$$

where $\Delta < \sigma > = < \sigma >_{130} - < \sigma >_{30}$
The above formula is justified by the facts that $\Delta < \sigma >$ are generally lower that 10% and the total flux intensities at $50°C$ and $30°C$ are identical (see table 1). With respect to the evolution of pure Maxwell averaged cross section with a $\frac{1}{v}$ behavior, this formula shows an agreement at the level of 0.5%.
Each averaged cross section is determined (see equation 2) from the integration of the differential cross sections (see the followings figures) tabulated in the ENDF-B6 library, on the base of 1000 simulated flux values over 10 neutron energy decades. The uncertainty on the averaged cross section, which is mainly correlated to the importance of the epithermal reaction rate and the number of generated simulated neutrons at these energies, can reach 9% for $^{242}Pu(n,\gamma)$, but is generally equal to 2% for the other isotopes.

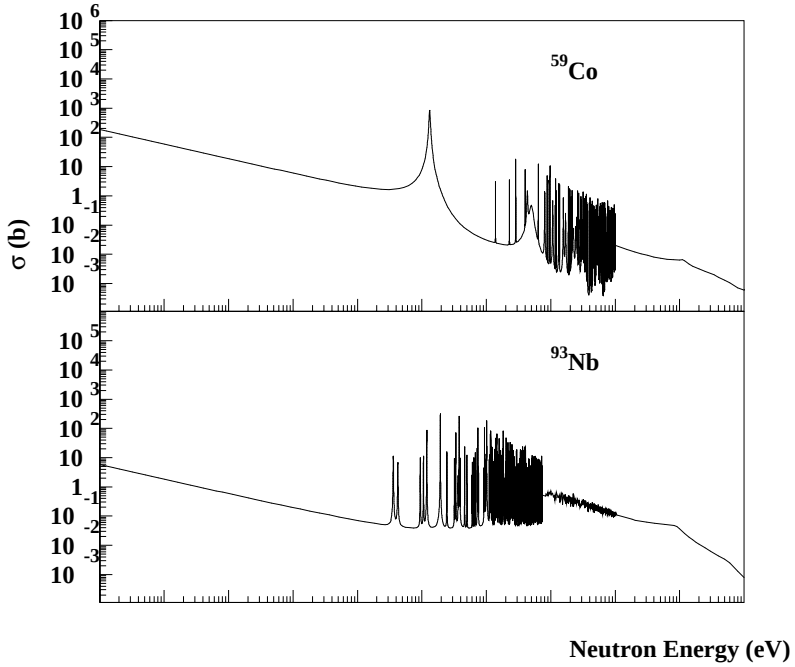
σ (b)
^{59}Co
^{93}Nb
Neutron Energy (eV)

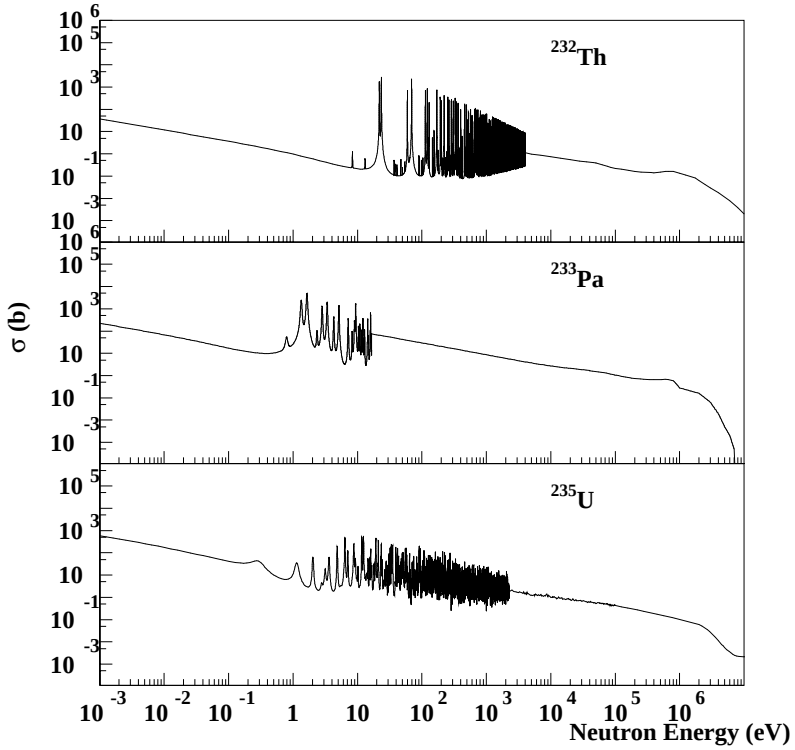
σ (b)
^{232}Th
^{233}Pa
^{235}U
Neutron Energy (eV)

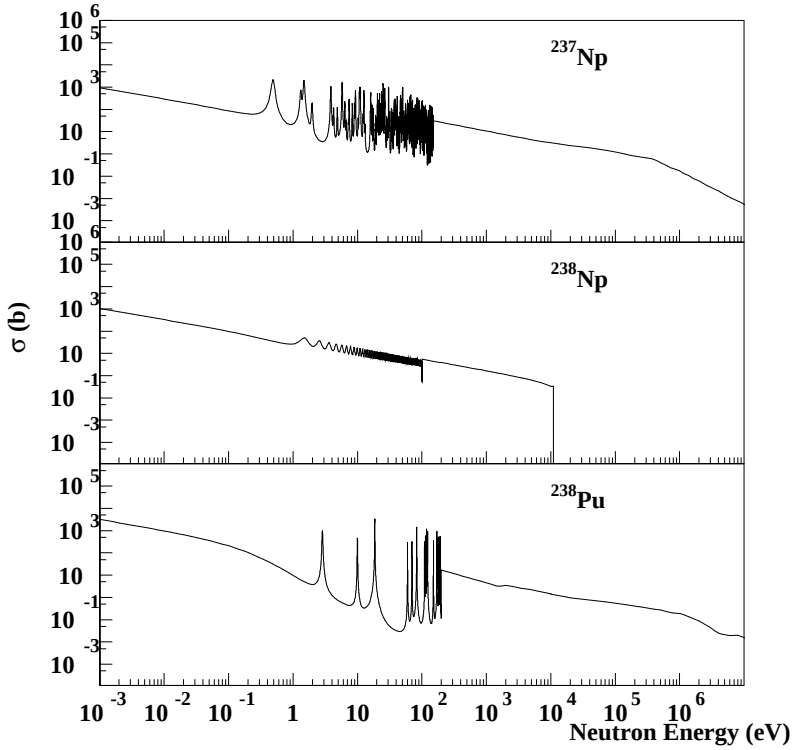
^{237}Np
^{238}Np
^{238}Pu
σ (b)
Neutron Energy (eV)

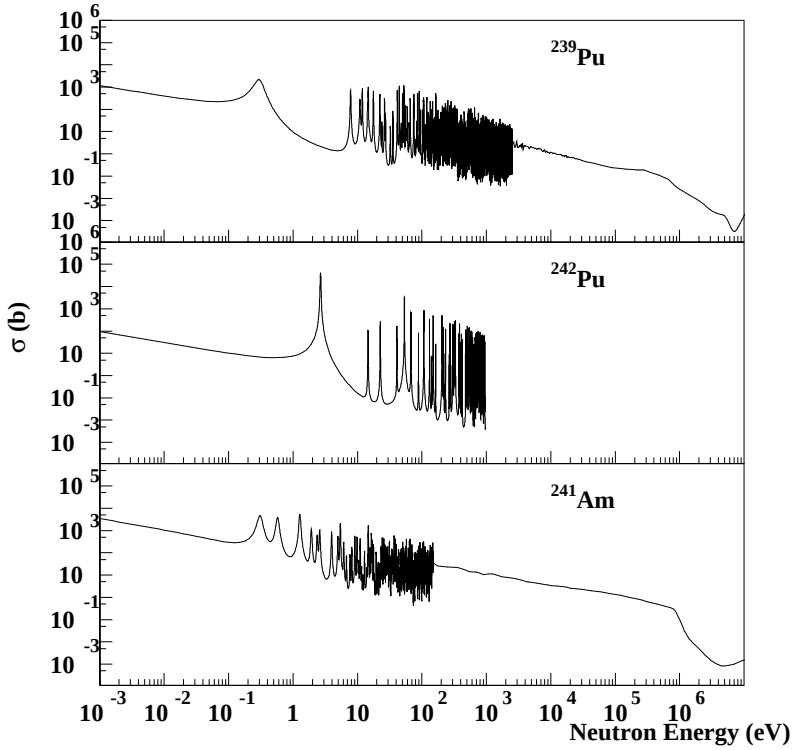
^{239}Pu
^{242}Pu
^{241}Am
σ (b)
Neutron Energy (eV)

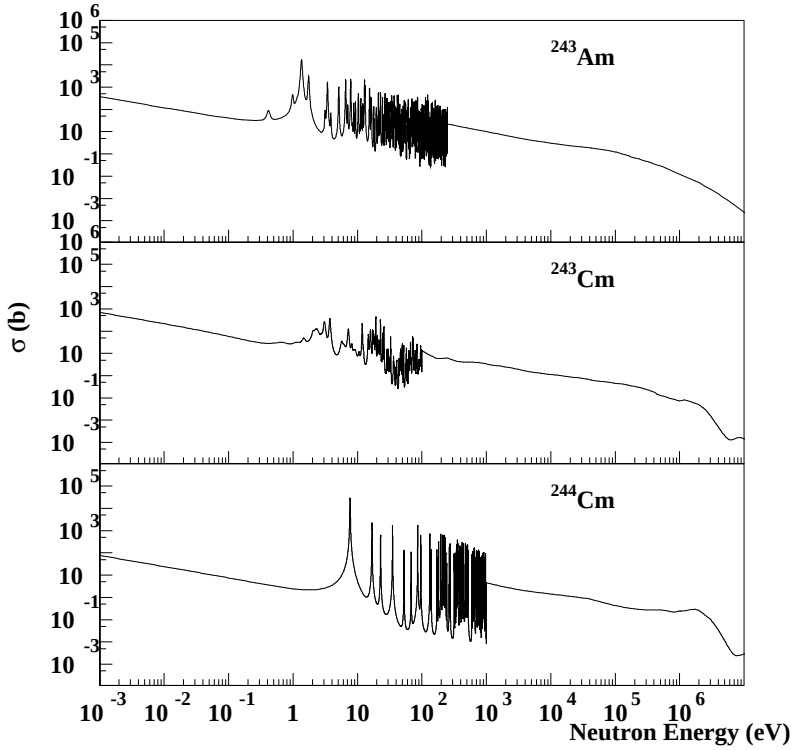
^{243}Am
^{243}Cm
^{244}Cm
σ (b)
Neutron Energy (eV)

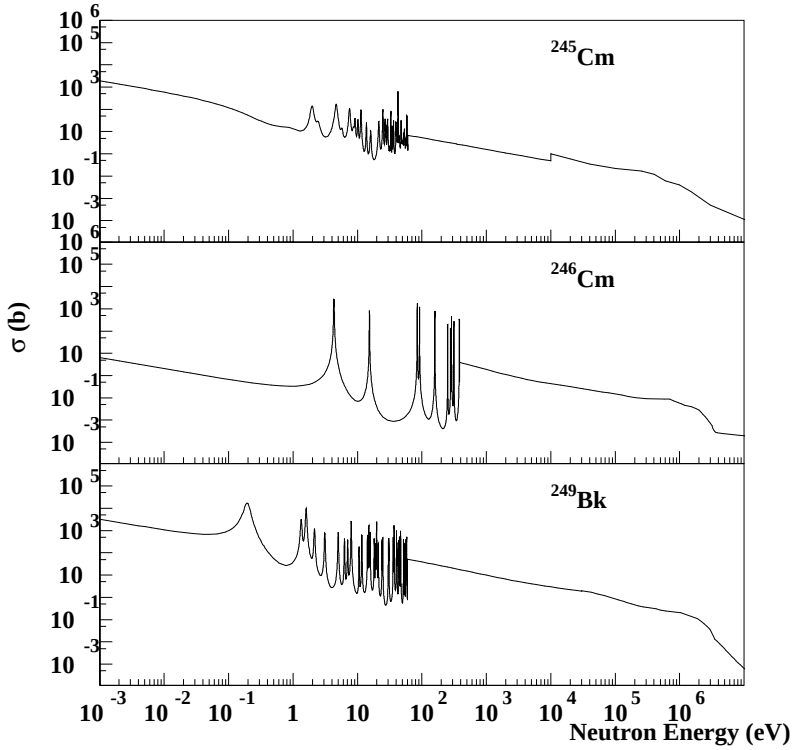
^{245}Cm
^{246}Cm
^{249}Bk
σ (b)
Neutron Energy (eV)

3 Results

3.1 Effect of the non-thermal component of the flux

For a exhaustive set of minor actinides, for which an experimental campaign of thermal neutron capture and fission cross sections has been initiated at ILL [3, 5], we have calculated (from equation 10) the averaged cross sections $< \sigma >_{50}$. For each irradiation position, we have determined the ratio with the corresponding tabulated cross sections σ_0 and σ_{Max}, respectively at $E_n = 0.0253\ eV$ and Maxwell averaged at $50°C$. In the last column of the table we recall the contribution of the thermal neutrons ($E_n < 1eV$) to the reaction rate R^{tot}. All these calculations have been performed using the differential cross sections tabulated in the ENDF-B6 [8] evaluated data bank, except for $^{233,234}Th$, ^{244}Am, ^{233}Pa, $^{243,244}Cm$ and ^{250}Bk for which we have used JENDL3.3 [9] evaluations. The first table is relative to capture cross sections, whereas the second one is for fission cross sections.

3.1.1 Capture cross sections

^{A}Z	Flux	$< \sigma >_{30}$	$< \sigma >_{130}$	$< \sigma >_{50}$	σ_0	σ_{Max}	$\frac{<\sigma>_{50}}{\sigma_0}$	$\frac{<\sigma>_{50}}{\sigma_{Max}}$	$\frac{R^{th}}{R^{tot}}$
	core	4.61	4.59	4.61			0.123	0.146	0.455
	V4(0)	27.36	24.22	26.73			0.717	0.845	0.962
	V4(25)	29.04	25.52	28.33			0.760	0.896	0.976
^{59}Co	V4(50)	31.51	27.67	30.74	37.30	31.62	0.824	0.972	0.992
	V4(75)	32.48	28.37	31.66			0.849	1.001	0.999
	V4(100)	32.68	28.50	31.84			0.854	1.007	1.000
	H9	31.86	28.06	31.10			0.834	0.984	0.996
	core	0.52	0.52	0.52			0.448	0.529	0.126
	V4(0)	0.94	0.84	0.92			0.791	0.934	0.873
	V4(25)	0.95	0.84	0.93			0.802	0.946	0.926
^{93}Nb	V4(50)	1.00	0.89	0.97	1.16	0.98	0.839	0.990	0.978
	V4(75)	1.01	0.89	0.99			0.850	1.003	0.998
	V4(100)	1.02	0.89	0.99			0.855	1.009	0.999
	H9	1.00	0.88	0.98			0.842	0.994	0.986
	core	3.28	3.26	3.28			0.442	0.525	0.124
	V4(0)	6.52	5.83	6.39			0.861	1.022	0.798
	V4(25)	6.41	5.77	6.28			0.847	1.006	0.875
^{232}Th	V4(50)	6.48	5.76	6.34	7.42	6.25	0.854	1.015	0.955
	V4(75)	6.46	5.60	6.29			0.848	1.007	0.995
	V4(100)	6.47	5.63	6.30			0.849	1.009	1.000
	H9	6.44	5.66	6.29			0.847	1.006	0.975

^{A}Z	Flux	$< \sigma >_{30}$	$< \sigma >_{130}$	$< \sigma >_{50}$	σ_0	σ_{Max}	$\frac{<\sigma>_{50}}{\sigma_0}$	$\frac{<\sigma>_{50}}{\sigma_{Max}}$	$\frac{R^{th}}{R^{tot}}$
	core	93.57	93.96	93.65			0.065	0.076	0.868
	V4(0)	1027.52	911.12	1004.24			0.692	0.820	0.993
	V4(25)	1104.57	971.11	1077.88			0.743	0.880	0.995
^{233}Th	V4(50)	1214.29	1059.28	1183.29	1450.58	1224.36	0.816	0.966	0.998
	V4(75)	1258.55	1099.62	1226.76			0.846	1.002	1.000
	V4(100)	1266.73	1104.59	1234.30			0.851	1.008	1.000
	H9	1230.95	1082.96	1201.35			0.828	0.981	0.999
	core	3.23	3.20	3.22			1.840	2.179	0.030
	V4(0)	2.58	2.41	2.55			1.453	1.722	0.477
	V4(25)	2.27	2.03	2.22			1.268	1.502	0.585
^{234}Th	V4(50)	1.77	1.60	1.73	1.75	1.48	0.990	1.173	0.828
	V4(75)	1.56	1.34	1.52			0.866	1.026	0.973
	V4(100)	1.54	1.33	1.50			0.857	1.015	0.991
	H9	1.67	1.49	1.63			0.933	1.106	0.888
	core	25.61	25.41	25.57			0.639	0.774	0.089
	V4(0)	41.79	37.84	41.00			1.025	1.240	0.660
	V4(25)	40.28	35.14	39.25			0.981	1.188	0.737
^{233}Pa	V4(50)	36.73	31.29	35.64	40.00	33.05	0.891	1.078	0.890
	V4(75)	34.53	29.23	33.47			0.837	1.013	0.981
	V4(100)	34.15	29.04	33.13			0.828	1.002	0.999
	H9	35.41	30.51	34.43			0.861	1.042	0.936
	core	6.36	6.41	6.37			0.139	0.160	0.439
	V4(0)	35.41	32.32	34.79			0.760	0.874	0.939
	V4(25)	37.34	33.69	36.61			0.800	0.919	0.958
^{233}U	V4(50)	39.96	35.75	39.12	45.77	39.83	0.855	0.982	0.985
	V4(75)	40.90	36.70	40.06			0.875	1.006	0.998
	V4(100)	41.09	36.80	40.24			0.879	1.010	1.000
	H9	40.29	36.36	39.50			0.863	0.992	0.991
	core	23.02	22.84	22.99			0.222	0.266	0.235
	V4(0)	81.06	75.27	79.90			0.772	0.924	0.881
	V4(25)	84.90	75.42	83.01			0.802	0.960	0.907
^{234}U	V4(50)	87.44	76.30	85.21	103.50	86.50	0.823	0.985	0.973
	V4(75)	88.53	76.74	86.17			0.833	0.996	0.998
	V4(100)	89.00	76.86	86.57			0.836	1.001	1.000
	H9	87.67	76.09	85.35			0.825	0.987	0.985
	core	8.97	8.91	8.96			0.090	0.108	0.567
	V4(0)	70.69	61.35	68.82			0.694	0.830	0.971
	V4(25)	75.47	64.72	73.32			0.739	0.885	0.981
^{235}U	V4(50)	82.27	70.14	79.85	99.20	82.87	0.805	0.963	0.994
	V4(75)	84.93	72.45	82.43			0.831	0.995	0.999
	V4(100)	85.47	72.71	82.92			0.836	1.001	1.000
	H9	83.19	71.50	80.85			0.815	0.976	0.996

^{A}Z	Flux	$< \sigma >_{30}$	$< \sigma >_{130}$	$< \sigma >_{50}$	σ_0	σ_{Max}	$\frac{<\sigma>_{50}}{\sigma_0}$	$\frac{<\sigma>_{50}}{\sigma_{Max}}$	$\frac{R^{th}}{R^{tot}}$
	core	9.55	9.48	9.53			1.857	2.197	0.031
	V4(0)	8.93	9.13	8.97			1.748	2.068	0.406
	V4(25)	7.25	8.03	7.41			1.443	1.707	0.538
^{236}U	V4(50)	5.57	6.57	5.77	5.13	4.34	1.123	1.329	0.773
	V4(75)	4.55	4.00	4.44			0.866	1.024	0.980
	V4(100)	4.49	3.93	4.38			0.853	1.009	1.000
	H9	5.49	4.82	5.36			1.044	1.235	0.794
	core	32.95	32.81	32.92			0.069	0.084	0.751
	V4(0)	333.40	292.48	325.22			0.683	0.829	0.987
	V4(25)	358.16	311.40	348.81			0.733	0.889	0.992
^{237}U	V4(50)	393.57	339.41	382.74	475.90	392.25	0.804	0.976	0.997
	V4(75)	407.88	352.37	396.78			0.834	1.012	1.000
	V4(100)	410.54	354.05	399.25			0.839	1.018	1.000
	H9	398.82	347.35	388.52			0.816	0.991	0.999
	core	6.84	6.81	6.84			2.504	2.953	0.023
	V4(0)	6.13	5.76	6.06			2.218	2.617	0.315
	V4(25)	5.15	5.07	5.13			1.880	2.218	0.404
^{238}U	V4(50)	3.26	3.01	3.21	2.73	2.31	1.176	1.387	0.703
	V4(75)	2.40	2.10	2.34			0.857	1.011	0.991
	V4(100)	2.40	2.09	2.34			0.856	1.009	0.999
	H9	3.03	2.73	2.97			1.088	1.283	0.767
	core	32.64	32.51	32.61			0.180	0.214	0.509
	V4(0)	141.04	125.60	137.95			0.761	0.907	0.940
	V4(25)	147.35	129.74	143.82			0.794	0.946	0.958
^{237}Np	V4(50)	154.63	136.04	150.91	181.20	152.10	0.833	0.992	0.986
	V4(75)	156.75	136.07	152.62			0.842	1.003	0.998
	V4(100)	157.19	136.29	153.01			0.844	1.006	1.000
	H9	155.11	136.25	151.34			0.835	0.995	0.991
	core	13.08	13.05	13.07			0.064	0.077	0.828
	V4(0)	143.09	125.82	139.63			0.685	0.817	0.991
	V4(25)	153.85	134.06	149.90			0.736	0.877	0.994
^{238}Np	V4(50)	169.25	146.35	164.67	203.70	170.87	0.808	0.964	0.998
	V4(75)	175.46	151.91	170.75			0.838	0.999	1.000
	V4(100)	176.63	152.63	171.83			0.844	1.006	1.000
	H9	171.56	149.69	167.18			0.821	0.978	0.999
	core	18.04	17.94	18.02			0.234	0.277	0.239
	V4(0)	60.80	54.55	59.55			0.773	0.914	0.890
	V4(25)	62.97	55.67	61.51			0.799	0.944	0.927
^{239}Np	V4(50)	65.89	57.77	64.27	77.00	65.13	0.835	0.987	0.977
	V4(75)	66.98	58.54	65.29			0.848	1.003	0.997
	V4(100)	67.28	58.63	65.55			0.851	1.006	0.999
	H9	66.24	58.47	64.68			0.840	0.993	0.985

^{A}Z	Flux	$<\sigma>_{30}$	$<\sigma>_{130}$	$<\sigma>_{50}$	σ_0	σ_{Max}	$\frac{<\sigma>_{50}}{\sigma_0}$	$\frac{<\sigma>_{50}}{\sigma_{Max}}$	$\frac{R^{th}}{R^{tot}}$
	core	29.43	28.64	29.27			0.052	0.064	0.844
	V4(0)	375.85	318.93	364.47			0.646	0.802	0.994
	V4(25)	405.89	340.63	392.84			0.697	0.865	0.996
^{238}Pu	V4(50)	449.20	374.15	434.19	564.00	454.31	0.770	0.956	0.999
	V4(75)	466.65	389.32	451.18			0.800	0.993	1.000
	V4(100)	470.00	391.43	454.29			0.805	1.000	1.000
	H9	455.39	383.55	441.02			0.782	0.971	0.999
	core	41.93	45.28	42.60			0.156	0.162	0.879
	V4(0)	246.37	251.99	247.50			0.904	0.939	0.991
	V4(25)	257.36	263.40	258.56			0.945	0.981	0.994
^{239}Pu	V4(50)	270.89	277.58	272.23	273.70	263.63	0.995	1.033	0.998
	V4(75)	273.70	282.10	275.38			1.006	1.045	1.000
	V4(100)	274.42	282.64	276.07			1.009	1.047	1.000
	H9	272.38	276.95	273.29			0.999	1.037	0.999
	core	209.47	208.75	209.32			0.719	0.832	0.183
	V4(0)	360.04	347.04	357.44			1.228	1.421	0.627
	V4(25)	345.62	302.20	336.93			1.158	1.339	0.685
^{240}Pu	V4(50)	299.39	255.26	290.56	291.00	251.54	0.998	1.155	0.843
	V4(75)	258.05	236.47	253.73			0.872	1.009	0.998
	V4(100)	258.51	233.17	253.44			0.871	1.008	1.000
	H9	278.19	244.42	271.44			0.933	1.079	0.917
	core	29.32	30.47	29.55			0.081	0.094	0.832
	V4(0)	266.58	243.72	262.01			0.720	0.834	0.990
	V4(25)	284.38	257.63	279.03			0.767	0.888	0.993
^{241}Pu	V4(50)	309.50	278.96	303.39	364.00	314.30	0.833	0.965	0.998
	V4(75)	318.47	287.96	312.37			0.858	0.994	1.000
	V4(100)	320.20	288.87	313.94			0.862	0.999	1.000
	H9	312.79	282.35	306.70			0.843	0.976	0.999
	core	34.55	34.31	34.50			1.788	2.106	0.034
	V4(0)	36.14	31.53	35.21			1.825	2.150	0.382
	V4(25)	30.33	29.66	30.19			1.564	1.843	0.489
^{242}Pu	V4(50)	23.35	22.46	23.17	19.30	16.38	1.201	1.415	0.699
	V4(75)	17.15	18.58	17.43			0.903	1.064	0.987
	V4(100)	17.02	14.99	16.62			0.861	1.014	1.000
	H9	19.87	16.99	19.30			1.000	1.178	0.832
	core	11.97	11.91	11.95			0.136	0.162	0.394
	V4(0)	65.64	57.92	64.10			0.727	0.868	0.933
	V4(25)	69.24	60.40	67.47			0.766	0.913	0.953
^{243}Pu	V4(50)	74.10	64.12	72.10	88.11	73.87	0.818	0.976	0.984
	V4(75)	75.80	65.63	73.77			0.837	0.999	0.999
	V4(100)	76.25	65.92	74.19			0.842	1.004	1.000
	H9	74.70	65.14	72.79			0.826	0.985	0.990

^{A}Z	Flux	$< \sigma >_{30}$	$< \sigma >_{130}$	$< \sigma >_{50}$	σ_0	σ_{Max}	$\frac{<\sigma>_{50}}{\sigma_0}$	$\frac{<\sigma>_{50}}{\sigma_{Max}}$	$\frac{R^{th}}{R^{tot}}$
	core	3.40	3.37	3.39			1.855	2.200	0.030
	V4(0)	2.73	2.62	2.71			1.479	1.754	0.470
	V4(25)	2.49	2.22	2.44			1.333	1.581	0.554
^{244}Pu	V4(50)	1.81	1.69	1.78	1.83	1.54	0.975	1.156	0.844
	V4(75)	1.63	1.47	1.60			0.874	1.037	0.969
	V4(100)	1.59	1.39	1.55			0.848	1.006	1.000
	H9	1.72	1.67	1.71			0.936	1.110	0.897
	core	89.59	91.38	89.95			0.145	0.171	0.736
	V4(0)	486.29	443.40	477.71			0.768	0.907	0.971
	V4(25)	507.74	461.33	498.45			0.801	0.946	0.981
^{241}Am	V4(50)	535.73	480.58	524.70	622.00	526.69	0.844	0.996	0.993
	V4(75)	541.43	485.33	530.21			0.852	1.007	0.999
	V4(100)	543.34	485.15	531.70			0.855	1.010	1.000
	H9	537.46	482.16	526.40			0.846	0.999	0.995
	core	14.76	14.72	14.75			0.058	0.070	0.898
	V4(0)	176.66	155.06	172.34			0.680	0.813	0.995
	V4(25)	190.31	165.55	185.36			0.731	0.874	0.997
$^{242gs}Am$	V4(50)	209.85	181.17	204.11	253.50	212.11	0.805	0.962	0.999
	V4(75)	217.79	188.31	211.90			0.836	0.999	1.000
	V4(100)	219.26	189.21	213.25			0.841	1.005	1.000
	H9	212.82	185.41	207.34			0.818	0.978	0.999
	core	99.73	104.99	100.78			0.074	0.080	0.947
	V4(0)	1072.38	1020.23	1061.95			0.781	0.840	0.997
	V4(25)	1152.20	1090.55	1139.87			0.839	0.901	0.998
^{242m}Am	V4(50)	1263.58	1188.11	1248.49	1359.00	1264.83	0.919	0.987	0.999
	V4(75)	1310.00	1236.18	1295.24			0.953	1.024	1.000
	V4(100)	1317.50	1240.19	1302.04			0.958	1.029	1.000
	H9	1282.65	1212.34	1268.59			0.933	1.003	1.000
	core	52.45	52.08	52.37			0.695	0.812	0.110
	V4(0)	85.45	78.45	84.05			1.115	1.303	0.642
	V4(25)	80.71	75.07	79.58			1.056	1.233	0.727
^{243}Am	V4(50)	73.37	67.38	72.18	75.35	64.52	0.958	1.119	0.873
	V4(75)	68.08	58.93	66.25			0.879	1.027	0.972
	V4(100)	66.55	58.93	65.03			0.863	1.008	1.000
	H9	69.39	63.31	68.18			0.905	1.057	0.935
	core	42.40	43.01	42.52			0.071	0.082	0.850
	V4(0)	437.24	394.21	428.64			0.714	0.828	0.992
	V4(25)	469.44	419.81	459.51			0.766	0.887	0.994
$^{244gs}Am$	V4(50)	515.01	457.05	503.42	600.20	517.91	0.839	0.972	0.998
	V4(75)	533.35	474.36	521.55			0.869	1.007	1.000
	V4(100)	536.50	476.08	524.41			0.874	1.013	1.000
	H9	521.97	466.55	510.89			0.851	0.986	0.999

^{A}Z	Flux	$<\sigma>_{30}$	$<\sigma>_{130}$	$<\sigma>_{50}$	σ_0	σ_{Max}	$\frac{<\sigma>_{50}}{\sigma_0}$	$\frac{<\sigma>_{50}}{\sigma_{Max}}$	$\frac{R^{th}}{R^{tot}}$
	core	36.14	37.62	36.44			0.091	0.098	0.825
	V4(0)	320.01	303.33	316.67			0.791	0.851	0.989
	V4(25)	342.28	322.26	338.28			0.845	0.909	0.992
^{244m}Am	V4(50)	373.15	348.96	368.32	400.13	372.24	0.920	0.989	0.997
	V4(75)	385.47	361.96	380.77			0.952	1.023	1.000
	V4(100)	387.02	362.33	382.08			0.955	1.026	1.000
	H9	377.98	354.62	373.31			0.933	1.003	0.998
	core	4.53	4.49	4.52			0.268	0.319	0.199
	V4(0)	13.32	11.72	13.00			0.769	0.916	0.887
	V4(25)	13.77	12.37	13.49			0.798	0.950	0.925
^{242}Cm	V4(50)	14.44	12.56	14.07	16.90	14.19	0.832	0.991	0.974
	V4(75)	14.67	12.67	14.27			0.844	1.005	0.996
	V4(100)	14.80	12.73	14.39			0.851	1.014	0.994
	H9	14.45	12.72	14.10			0.834	0.994	0.988
	core	12.29	12.20	12.27			0.094	0.114	0.563
	V4(0)	92.85	81.15	90.51			0.695	0.839	0.966
	V4(25)	99.00	85.57	96.31			0.740	0.893	0.977
^{243}Cm	V4(50)	107.68	92.31	104.61	130.20	107.82	0.803	0.970	0.992
	V4(75)	111.03	95.21	107.86			0.828	1.000	0.999
	V4(100)	111.71	95.61	108.49			0.833	1.006	1.000
	H9	108.82	94.22	105.90			0.813	0.982	0.996
	core	18.91	18.76	18.88			1.250	1.484	0.044
	V4(0)	20.87	17.54	20.21			1.337	1.588	0.507
	V4(25)	18.95	16.35	18.43			1.220	1.448	0.602
^{244}Cm	V4(50)	14.79	12.49	14.33	15.11	12.72	0.948	1.126	0.851
	V4(75)	13.50	11.41	13.08			0.866	1.028	0.968
	V4(100)	13.17	11.44	12.83			0.849	1.008	0.999
	H9	14.02	12.52	13.72			0.908	1.078	0.911
	core	17.60	17.02	17.49			0.051	0.063	0.841
	V4(0)	226.88	191.36	219.78			0.639	0.798	0.993
	V4(25)	244.90	204.18	236.76			0.689	0.859	0.995
^{245}Cm	V4(50)	271.04	224.24	261.68	343.80	275.54	0.761	0.950	0.998
	V4(75)	281.56	233.25	271.90			0.791	0.987	1.000
	V4(100)	283.59	234.51	273.77			0.796	0.994	1.000
	H9	274.75	229.94	265.79			0.773	0.965	0.999
	core	3.14	3.09	3.13			2.398	2.820	0.024
	V4(0)	2.52	2.32	2.48			1.901	2.236	0.368
	V4(25)	2.16	1.89	2.11			1.616	1.900	0.461
^{246}Cm	V4(50)	1.50	1.31	1.46	1.30	1.11	1.121	1.318	0.733
	V4(75)	1.16	1.01	1.13			0.866	1.019	0.983
	V4(100)	1.15	1.01	1.12			0.858	1.010	1.000
	H9	1.37	1.27	1.35			1.033	1.215	0.815

^{A}Z	Flux	$<\sigma>_{30}$	$<\sigma>_{130}$	$<\sigma>_{50}$	σ_0	σ_{Max}	$\frac{<\sigma>_{50}}{\sigma_0}$	$\frac{<\sigma>_{50}}{\sigma_{Max}}$	$\frac{R^{th}}{R^{tot}}$
	core	15.69	15.71	15.70			0.270	0.323	0.796
	V4(0)	51.35	47.22	50.53			0.868	1.038	0.964
	V4(25)	52.06	48.58	51.36			0.883	1.055	0.975
^{247}Cm	V4(50)	52.78	46.90	51.60	58.20	48.67	0.887	1.060	0.990
	V4(75)	52.11	47.23	51.13			0.879	1.051	0.999
	V4(100)	52.20	47.04	51.17			0.879	1.051	1.000
	H9	52.31	47.61	51.37			0.883	1.055	0.995
	core	7.18	7.10	7.16			2.930	3.462	0.019
	V4(0)	5.74	5.15	5.62			2.299	2.716	0.300
	V4(25)	4.76	3.92	4.59			1.877	2.218	0.390
^{248}Cm	V4(50)	2.90	2.68	2.85	2.44	2.07	1.167	1.378	0.707
	V4(75)	2.32	1.87	2.23			0.910	1.075	0.918
	V4(100)	2.14	1.87	2.09			0.853	1.008	1.000
	H9	2.90	3.03	2.93			1.198	1.415	0.716
	core	190.15	228.05	197.74			0.265	0.212	0.841
	V4(0)	928.47	1204.52	983.68			1.317	1.055	0.979
	V4(25)	958.83	1266.93	1020.45			1.366	1.094	0.986
^{249}Bk	V4(50)	987.64	1312.20	1052.56	747.00	932.43	1.409	1.129	0.995
	V4(75)	981.61	1383.62	1062.01			1.422	1.139	0.999
	V4(100)	974.83	1336.65	1047.20			1.402	1.123	1.000
	H9	990.21	1308.88	1053.94			1.411	1.130	0.997
	core	20.21	19.53	20.07			0.057	0.071	0.726
	V4(0)	232.88	195.00	225.30			0.638	0.800	0.987
	V4(25)	250.96	207.36	242.24			0.686	0.860	0.991
^{250}Bk	V4(50)	277.11	227.21	267.13	353.27	281.72	0.756	0.948	0.997
	V4(75)	287.48	236.05	277.20			0.785	0.984	1.000
	V4(100)	289.58	237.29	279.12			0.790	0.991	1.000
	H9	280.75	232.81	271.16			0.768	0.963	0.998
	core	38.93	38.59	38.86			0.078	0.095	0.917
	V4(0)	350.03	302.88	340.60			0.683	0.833	0.995
	V4(25)	373.79	321.57	363.34			0.728	0.888	0.997
^{249}Cf	V4(50)	408.20	346.55	395.87	499.00	409.07	0.793	0.968	0.999
	V4(75)	420.84	357.83	408.24			0.818	0.998	1.000
	V4(100)	423.48	359.13	410.61			0.823	1.004	1.000
	H9	412.62	353.46	400.79			0.803	0.980	0.999
	core	363.62	364.87	363.87			0.225	0.263	0.974
	V4(0)	1389.10	1256.51	1362.58			0.844	0.983	0.996
	V4(25)	1396.60	1295.71	1376.42			0.852	0.993	0.997
^{250}Cf	V4(50)	1441.97	1288.54	1411.28	1615.00	1385.79	0.874	1.018	0.999
	V4(75)	1430.50	1275.22	1399.44			0.867	1.010	1.000
	V4(100)	1433.92	1265.48	1400.23			0.867	1.010	1.000
	H9	1441.46	1269.98	1407.16			0.871	1.015	0.999

^{A}Z	Flux	$<\sigma>_{30}$	$<\sigma>_{130}$	$<\sigma>_{50}$	σ_0	σ_{Max}	$\frac{<\sigma>_{50}}{\sigma_0}$	$\frac{<\sigma>_{50}}{\sigma_{Max}}$	$\frac{R^{th}}{R^{tot}}$
	core	187.85	187.97	187.87			0.066	0.078	0.966
	V4(0)	2029.71	1787.66	1981.30			0.691	0.822	0.998
	V4(25)	2178.57	1906.10	2124.08			0.741	0.881	0.999
^{251}Cf	V4(50)	2392.78	2072.91	2328.81	2867.00	2411.55	0.812	0.966	1.000
	V4(75)	2476.74	2149.16	2411.22			0.841	1.000	1.000
	V4(100)	2492.83	2158.51	2425.97			0.846	1.006	1.000
	H9	2423.89	2118.24	2362.76			0.824	0.980	1.000
	core	2.61	2.59	2.60			0.126	0.151	0.415
	V4(0)	14.97	13.22	14.62			0.710	0.848	0.956
	V4(25)	15.86	13.82	15.45			0.750	0.896	0.973
^{252}Cf	V4(50)	17.19	14.92	16.74	20.60	17.24	0.813	0.971	0.992
	V4(75)	17.72	15.33	17.24			0.837	1.000	1.000
	V4(100)	17.83	15.40	17.35			0.842	1.006	1.000
	H9	17.39	15.15	16.94			0.822	0.983	0.995

3.1.2 Fission cross sections

^{A}Z	Flux	$<\sigma>_{30}$	$<\sigma>_{130}$	$<\sigma>_{50}$	σ_0	σ_M	$\frac{<\sigma>_{50}}{\sigma_0}$	$\frac{<\sigma>_{50}}{\sigma_M}$	$\frac{N_r^{th}}{N_r^{tot}}$
	core	49.29	49.30	49.29			0.093	0.111	0.609
	V4(0)	381.67	338.98	373.13			0.706	0.840	0.972
	V4(25)	407.20	357.85	397.33			0.752	0.894	0.981
^{233}U	V4(50)	443.08	386.27	431.71	528.48	444.31	0.817	0.972	0.994
	V4(75)	457.06	398.68	445.38			0.843	1.002	0.999
	V4(100)	459.83	400.38	447.94			0.848	1.008	1.000
	H9	448.21	393.84	437.34			0.828	0.984	0.996
	core	37.55	37.31	37.50			0.064	0.077	0.805
	V4(0)	405.92	353.82	395.50			0.675	0.814	0.992
	V4(25)	436.62	376.90	424.68			0.725	0.874	0.994
^{235}U	V4(50)	480.59	411.82	466.83	586.00	485.74	0.797	0.961	0.998
	V4(75)	498.33	427.55	484.17			0.826	0.997	1.000
	V4(100)	501.71	429.58	487.29			0.832	1.003	1.000
	H9	487.12	421.18	473.93			0.809	0.976	0.999
	core	127.19	126.93	127.14			0.062	0.074	0.849
	V4(0)	1427.84	1255.21	1393.31			0.685	0.816	0.992
	V4(25)	1535.95	1337.98	1496.36			0.735	0.876	0.995
^{238}Np	V4(50)	1690.49	1461.37	1644.67	2035.00	1707.71	0.808	0.963	0.998
	V4(75)	1752.95	1517.31	1705.82			0.838	0.999	1.000
	V4(100)	1764.61	1524.61	1716.61			0.844	1.005	1.000
	H9	1713.73	1494.94	1669.97			0.821	0.978	0.999

^{A}Z	Flux	$<\sigma>_{30}$	$<\sigma>_{130}$	$<\sigma>_{50}$	σ_0	σ_{Max}	$\frac{<\sigma>_{50}}{\sigma_0}$	$\frac{<\sigma>_{50}}{\sigma_{Max}}$	$\frac{R^{th}}{R^{tot}}$
	core	78.09	82.41	78.95			0.105	0.118	0.897
	V4(0)	593.52	565.77	587.97			0.782	0.878	0.994
	V4(25)	628.46	596.16	622.00			0.828	0.929	0.996
^{239}Pu	V4(50)	675.45	637.94	667.95	751.40	669.56	0.889	0.998	0.999
	V4(75)	690.66	653.84	683.30			0.909	1.021	1.000
	V4(100)	693.82	655.93	686.24			0.913	1.025	1.000
	H9	681.65	642.87	673.89			0.897	1.006	0.999
	core	85.56	89.42	86.34			0.085	0.097	0.812
	V4(0)	767.62	717.52	757.60			0.748	0.848	0.989
	V4(25)	819.66	760.48	807.82			0.798	0.904	0.993
^{241}Pu	V4(50)	892.69	823.95	878.94	1012.33	893.67	0.868	0.984	0.998
	V4(75)	920.53	852.67	906.95			0.896	1.015	1.000
	V4(100)	925.41	855.30	911.39			0.900	1.020	1.000
	H9	903.72	835.89	890.15			0.879	0.996	0.999
	core	24.41	24.30	24.39			0.134	0.160	0.397
	V4(0)	134.99	119.11	131.82			0.727	0.867	0.934
	V4(25)	142.46	124.25	138.81			0.765	0.913	0.954
^{243}Pu	V4(50)	152.52	131.98	148.42	181.40	152.10	0.818	0.976	0.984
	V4(75)	156.05	135.11	151.87			0.837	0.998	0.999
	V4(100)	156.99	135.70	152.73			0.842	1.004	1.000
	H9	153.77	134.10	149.83			0.826	0.985	0.990
	core	131.71	131.39	131.64			0.058	0.069	0.906
	V4(0)	1589.68	1395.33	1550.81			0.680	0.813	0.996
	V4(25)	1712.66	1489.83	1668.09			0.731	0.874	0.997
$^{242gs}Am$	V4(50)	1888.66	1630.56	1837.04	2281.00	1908.67	0.805	0.962	0.999
	V4(75)	1960.24	1694.92	1907.18			0.836	0.999	1.000
	V4(100)	1973.49	1703.04	1919.40			0.841	1.006	1.000
	H9	1915.46	1668.75	1866.12			0.818	0.978	0.999
	core	499.86	524.41	504.77			0.075	0.081	0.926
	V4(0)	5264.98	4992.13	5210.41			0.778	0.840	0.996
	V4(25)	5654.42	5333.18	5590.17			0.834	0.901	0.997
^{242m}Am	V4(50)	6198.09	5807.05	6119.88	6700.00	6206.03	0.913	0.986	0.999
	V4(75)	6423.77	6039.43	6346.90			0.947	1.023	1.000
	V4(100)	6460.57	6059.44	6380.34			0.952	1.028	1.000
	H9	6290.31	5925.19	6217.29			0.928	1.002	0.999
	core	165.90	168.68	166.46			0.072	0.083	0.847
	V4(0)	1687.76	1527.60	1655.73			0.720	0.829	0.991
	V4(25)	1811.52	1626.47	1774.51			0.771	0.889	0.994
$^{244gs}Am$	V4(50)	1986.44	1770.02	1943.16	2300.79	1996.98	0.845	0.973	0.998
	V4(75)	2056.78	1836.96	2012.82			0.875	1.008	1.000
	V4(100)	2068.63	1843.24	2023.55			0.880	1.013	1.000
	H9	2013.20	1806.17	1971.79			0.857	0.987	0.999

^{A}Z	Flux	$<\sigma>_{30}$	$<\sigma>_{130}$	$<\sigma>_{50}$	σ_0	σ_{Max}	$\frac{<\sigma>_{50}}{\sigma_0}$	$\frac{<\sigma>_{50}}{\sigma_{Max}}$	$\frac{R^{th}}{R^{tot}}$
	core	144.09	149.88	145.24			0.091	0.098	0.824
	V4(0)	1277.84	1209.89	1264.25			0.790	0.850	0.989
	V4(25)	1366.89	1285.48	1350.61			0.844	0.908	0.992
^{244m}Am	V4(50)	1490.39	1392.15	1470.74	1600.66	1487.35	0.919	0.989	0.997
	V4(75)	1539.67	1444.04	1520.54			0.950	1.022	1.000
	V4(100)	1545.95	1445.59	1525.88			0.953	1.026	1.000
	H9	1509.68	1414.90	1490.72			0.931	1.002	0.998
	core	75.04	75.09	75.05			0.121	0.143	0.512
	V4(0)	459.21	410.46	449.46			0.727	0.858	0.951
	V4(25)	485.58	429.40	474.34			0.768	0.906	0.967
^{243}Cm	V4(50)	522.02	457.76	509.16	618.00	523.84	0.824	0.972	0.988
	V4(75)	535.44	469.70	522.29			0.845	0.997	0.998
	V4(100)	538.06	471.27	524.70			0.849	1.002	1.000
	H9	526.55	465.92	514.42			0.832	0.982	0.993
	core	120.87	117.61	120.22			0.054	0.067	0.834
	V4(0)	1486.07	1261.16	1441.09			0.646	0.801	0.993
	V4(25)	1602.42	1345.16	1550.97			0.695	0.863	0.995
^{245}Cm	V4(50)	1770.92	1474.72	1711.68	2231.00	1798.19	0.767	0.952	0.998
	V4(75)	1838.79	1533.18	1777.67			0.797	0.989	1.000
	V4(100)	1851.76	1541.22	1789.65			0.802	0.995	1.000
	H9	1795.05	1511.47	1738.33			0.779	0.967	0.999
	core	24.22	24.24	24.22			0.290	0.352	0.775
	V4(0)	74.54	68.67	73.37			0.879	1.066	0.964
	V4(25)	75.39	70.64	74.44			0.892	1.082	0.975
^{247}Cm	V4(50)	76.12	67.78	74.45	83.47	68.82	0.892	1.082	0.990
	V4(75)	74.97	68.16	73.61			0.882	1.070	0.999
	V4(100)	75.08	67.85	73.63			0.882	1.070	1.000
	H9	75.37	68.79	74.05			0.887	1.076	0.995
	core	144.01	143.33	143.87			0.088	0.106	0.910
	V4(0)	1171.84	1021.37	1141.75			0.696	0.843	0.995
	V4(25)	1247.02	1082.24	1214.06			0.740	0.896	0.996
^{249}Cf	V4(50)	1356.00	1159.59	1316.72	1641.00	1354.36	0.802	0.972	0.999
	V4(75)	1394.70	1194.57	1354.67			0.826	1.000	1.000
	V4(100)	1403.00	1198.34	1362.07			0.830	1.006	1.000
	H9	1369.43	1180.94	1331.73			0.812	0.983	0.999
	core	403.18	404.28	403.40			0.076	0.090	0.959
	V4(0)	3835.11	3390.91	3746.27			0.702	0.832	0.997
	V4(25)	4100.35	3607.70	4001.82			0.750	0.888	0.998
^{251}Cf	V4(50)	4483.25	3898.82	4366.36	5333.00	4504.99	0.819	0.969	0.999
	V4(75)	4627.95	4031.43	4508.65			0.845	1.001	1.000
	V4(100)	4656.72	4047.08	4534.79			0.850	1.007	1.000
	H9	4536.30	3977.70	4424.58			0.830	0.982	1.000

3.2 Effect of sample temperature

In order to assess the effect of Doppler broadening due to the temperature of the samples, we present in table 4 averaged cross sections for some isotopes, calculated at 300° K (normal analysis) and 600° K (temperature of the samples during irradiation in H9). In both cases, temperature of the moderator is fixed at $300°K$, but calculations performed with $T_n = 400°\ K$ give the same conclusions.
Except for some extreme cases like ^{242}Pu capture cross section, which show a huge resonance orders of magnitude above the thermal value, the temperature of the samples in H9 is expected to play a negligible role for the majority of the isotopes studied. Same conclusions are expected in V4 where sample temperatures are estimated smaller ($T_{V4} < 420°K$) than in H9. We justify thus our study based on calculations of averaged cross sections at a unique sample temperatures of 300° K.

isotope	$< \sigma_c >^{300K}$	$< \sigma_c >^{600K}$	R_{300}^{600}
^{59}Co	31.8	31.8	1
^{241}Am	540	540	1
^{243}Am	70.6	70.4	0.997
^{242}Pu	18.2	18.6	1.022

Table 4: *Averaged capture cross sections for sample temperatures* $300°K$ *and* $600°K$. *In both cases, the temperature of neutron thermalization is set to* $300°K$.

4 Conclusions

We have performed an exhaustive analysis of the impact of the non-Maxwellian component of the neutron flux at ILL on the measurement of thermal neutron cross sections. This study is based on MCNP simulations of the HFR core providing calculated flux distributions at various irradiation positions. Averaged cross sections have been calculated on the basis of differential ENDF-BVI cross sections and compared to the thermal σ_0 and Maxwell averaged $< \sigma >_{50}$ cross sections. The results of this study show an agreement (at the level of a few %) between averaged and Maxwell averaged cross sections, for a wide set of minor actinides, in irradiation positions V4(50) to V4(100) and H9. However, for some actinides for which a huge resonance is reported closed to the thermal region (ex: $\sigma_c(^{242}Pu)$ or $\sigma_c(^{238}U)$), discrepancy can reach more than 20%, even for irradiation positions presenting few percents of non-thermal neutrons.
On the contrary, it has been shown that non-thermal neutron don't contribute to more than 5% to the fission rates in H9 and V4 or fissile actinides, which implies that the measured fission cross sections are representative of Maxwell averaged fission cross sections.
As an example, we present in table 5 some Correction Factors to be applied to the measured capture cross sections in H9 [1, 2], in order to derive the Maxwell averaged and thermal cross sections.

isotope X	$\Lambda_{Max}(X)$	$\Lambda_{Max}(^{59}Co)/\Lambda_{Max}(X)$	$\Lambda_0(X)$	$\Lambda_0(^{59}Co)/\Lambda_0(X)$
^{241}Am	0.999	**0.982**	0.846	**0.982**
^{243}Am	1.057	**0.928**	0.905	**0.918**
^{242}Pu	1.178	**0.833**	1.000	**0.831**

Table 5: *Example of correction factors to be applied for some measured capture cross sections in H9.* $\Lambda_{Max}(^{59}Co) = 0.981$ *and* $\Lambda_0(^{59}Co) = 0.831$

References

[1] G. Fioni, M. Cribier, F. Marie & al., *Incineration of* ^{241}Am *induced by thermal neutrons*, Nucl. Phys. **A 693** (2001) 546-564

[2] F. Marie & al., *Measurement of neutron capture cross sections relevant for nuclear waste transmutation by alpha and gamma spectroscopy*, Proc of the 11^{th} International Symposium on Capture Gamma-ray Spectroscopy and Related Topics, Prague, Czech Republic 2-6 sept 2002, in press

[3] F. Marie & al. "*Mesures Integrales des Sections Efficaces de capture et Fission d'Actinides*, DAPNIA-SPhN-00-50, CEA/Saclay (2000).

[4] D. Ridikas & al., "*On the fuel cycle and neutron fluxes of the high flux reactor at ILL Grenoble*", Proc. of the 5^{th} Int. Specialist's Meeting SATIF-5, OECD/NEA,-Paris(2000), pg 383.

[5] F. Marie & al. Internal Report at of the DAPNIA/SPhN CSTS (16 dec 2002)

[6] O. Deruelle, "*Mise au point d'un système de spectroscopie pour mesurer des sections efficaces neutroniques applicables à un possible développement du nucéaire comme source d'énergie*", Thèse de doctorat, DAPNIA-02-06-T (2002)

[7] M. Fadil, "*Mise au point d'une méthodologie innovante pour la mesure du potentiel d'incinération d'actinides mineurs sous des sources très intenses de neutrons, dans la perspective de la transmutation des déchets nucléaires*", Thèse de doctorat, DAPNIA-03-01-T (2003)

[8] http://www-nds.iaea.or.at/endf/endfframe.html, (upd Jully 2000)

[9] http://wwwndc.tokai.jaeri.go.jp/jendl/j33/j33.html, (upd Dec 2002)